Volume 13 | Number 7 | 31 March 2026

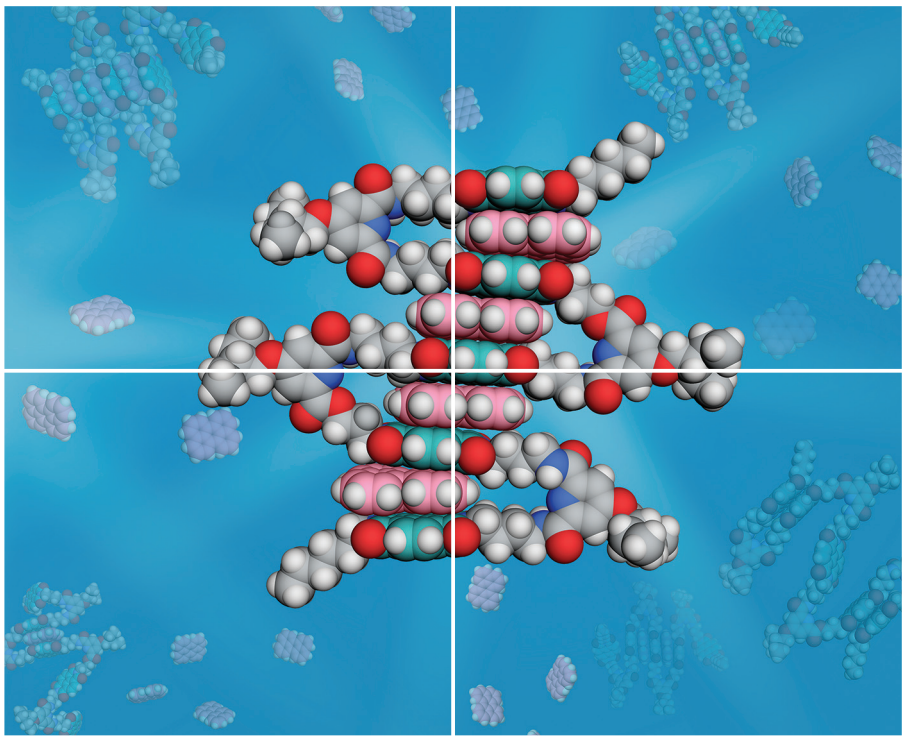

ORGANIC CHEMISTRY

FRONTIERS

CCS 中国化学会 CHINESE CHEMICAL SOCIETY

SIOC 1950

ROYAL SOCIETY OF CHEMISTRY

rsc.li/frontiers-organic

ORGANIC CHEMISTRY FRONTIERS

RESEARCH ARTICLE

View Article Online
View Journal | View Issue

Cite this: *Org. Chem. Front.*, 2026, **13**, 1986

Guest-dependent folding and tunable charge transfer of an NDI-pentamer

Dhanyashree Das, Dhrubajyoti Talukdar and Bappaditya Gole *

We present a covalently linked, electroactive, conformationally flexible naphthalene diimide (NDI) pentamer exhibiting unprecedented 10-electron reduction, solvent-dependent folding, and guest-induced tunable charge-transfer (CT). In dichloromethane and chloroform, the oligomer adopts a partially folded state, displaying bright excimer emission at 500 nm. The addition of methyl cyclohexane promotes ordered, long-range folding, thereby enhancing excimer emission. Conversely, the addition of toluene causes folding but quenches the excimer emission while inducing a distinct CT emission. Furthermore, various polyaromatic donors such as anthracene, triphenylene, pyrene, perylene, *etc.*, promote folding by intercalating between NDI layers, forming a long-range alternate donor–acceptor stack with tunable CT absorption. The estimation of the association constant (K_a) revealed that the strength of CT complexation depends on the donor ability of the guests, with perylene showing the highest association constant. Interestingly, sequential addition of two different donors produces dual CT bands, resulting in broad visible light absorption. This study demonstrates a rare example of guest-dependent tunable CT-driven folding of a flexible multidecker NDI system, offering new insights into the guest-mediated conformational control of foldamers and an approach towards ordered π-stacked materials.

Received 15th January 2026,
Accepted 12th February 2026

DOI: 10.1039/d6qo00055j

rsc.li/frontiers-organic

Introduction

Co-facial stacking of extended aromatic chromophores has emerged as a promising approach for constructing supramolecular self-assembled functional materials.[1–9] Such assemblies exhibit unique optical and electronic properties that are inaccessible to their monomeric counterparts. The precise alignment of the chromophores promotes extended orbital interaction, thereby facilitating charge transport and making them attractive candidates for efficient light harvesting and high-performance conductive materials in artificial photosynthetic systems.[10–15] However, unlike natural light-harvesting complexes, where protein scaffolds ensure precise organization of chromophores to facilitate efficient photoinduced charge separation and transport, artificial assemblies rely on various non-covalent interactions to achieve long-range order.[16–22] To elucidate the fundamental interactions among chromophores that result in their function, well-defined self-assembled aggregates with precise control over arrangement and size are desirable. Yet, conventional aggregations often suffer from uncontrolled growth and structural ambiguity due to their intrinsic dynamic nature.[23] Thus, this remains a persistent obstacle to their broader application.

An alternate emerging strategy involves the use of foldamer-based architectures, in which a defined number of chromophores are covalently linked through carefully designed turn units that direct hierarchical folding into multilayered π-stacks reminiscent of β-sheets in proteins.[24–31] Their predictable folding behaviour affords long-range order within discrete stacks, enabling tunable photophysical properties suitable for optoelectronic applications.[32–42] Recent examples include merocyanine foldamers that display panchromatic light absorption across the solar spectrum and perylene bisimide (PBI) tetramers exhibiting stepwise photoinduced charge hopping between terminal donor and acceptor units.[10,43] Despite these advances, controlling their folding in solution remains a major challenge. While rigid, conformationally locked oligomers ensure predictable structures, flexible systems are inherently dynamic, populating both folded and unfolded conformers. Seminal reports have shown that oligomers containing strongly dipolar chromophores such as merocyanine dyes exhibit solvent-dependent hierarchical folding, progressing from dimers to pentamers and eventually to extended aggregates.[44,45] Solvent polarity thus modulates the energy landscape between partially folded and fully stacked states, offering a means to control conformation and function.

Among the various chromophores considered in this direction, naphthalene diimide (NDI) is a promising candidate due

Biomimetic Supramolecular Chemistry Laboratory, Department of Chemistry, School of Natural Sciences, Shiv Nadar Institution of Eminence Deemed to be University, Greater Noida, Uttar Pradesh 201314, India. E-mail: bappaditya.gole@snu.edu.in

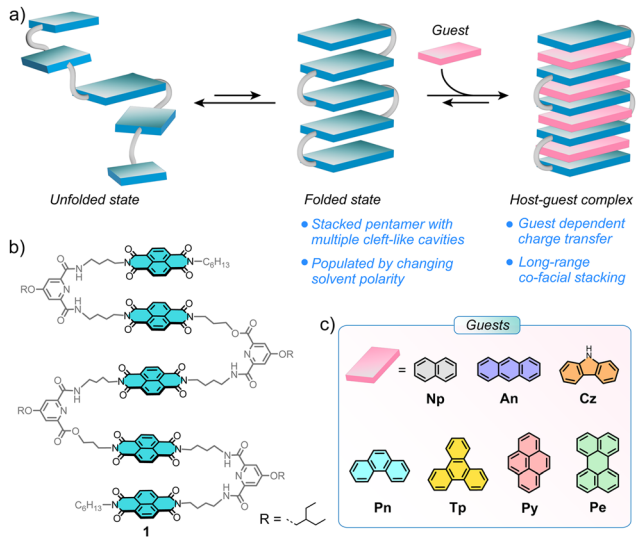

Fig. 1 (a) Schematic representation of the dynamic folded and unfolded states of the dye-appended oligomer. The presence of flexible turn units endows the dominant unfolded state in solution. An ordered folded state can be induced either by adding nonpolar solvents or by introducing electronically complementary polyaromatic donors, which intercalate to form donor–acceptor arrays through charge-transfer (CT) interactions. The CT response can be tuned by employing different donor guests. (b) Molecular structure of NDI-pentamer **1**. (c) Planar polyaromatic donors used in this study.

to its electron–acceptor properties and versatile optical and electrochemical properties, enabling its widespread applications in optoelectronics, photovoltaics, and conductive materials.[41,46–57] While self-assembled NDI monomers have been extensively studied in the past, reports on covalently linked NDI oligomers with long-range order remain limited.[58–65] Matile and co-workers demonstrated a tetrameric NDI foldamer with remarkable catalytic activity arising from synergistic π–π and anion–π interactions.[38] Takeuchi and co-workers recently reported discrete multi-decker NDI oligomers capable of multielectron reduction.[66] The relatively rigid conformation of these systems allows predictable stacking geometries; however, controlling the folding of flexible NDI oligomers remains an enduring challenge. We envisioned that CT interactions between electron-rich donors and electron-deficient NDI motifs could generate directional co-facial stacking stabilized by electronic complementarity (Fig. 1a).[67] These interactions may reinforce folding of the oligomer and long-range alternate donor–acceptor order, endowing materials with new optoelectronic functions such as colour tuning, photoinduced electron transfer, and exciton coupling.

Herein, we report the synthesis of a covalently linked, discrete, conformationally flexible NDI pentamer (**1**) designed to investigate its folding behavior and tunable CT interactions with polyaromatic donors in solution (Fig. 1). The oligomer exhibits conformational dynamics, existing predominantly in a partially folded state in dichloromethane and chloroform, with a bright excimer emission at 500 nm. An ordered folded state is achieved by the gradual addition of nonpolar solvents such as methylcyclohexane (MCH) and toluene. Notably, the addition of MCH enhances excimer emission, validating the reinforced folding process. In contrast, toluene quenches the excimer emission while inducing a CT emission. Furthermore, oligomer **1** exhibits tunable CT behavior that depends on the nature of the polyaromatic donor. These donor guests facilitate the folding of **1** by intercalating between the electron-deficient NDI sheets to form a long-range, alternate donor–acceptor stack. The association strength of these polyaromatic guests with **1** is primarily governed by their electron-donating ability, with perylene displaying the highest affinity. Additionally, sequential addition of two guests provides double CT bands, resulting in broad visible absorption. To the best of our knowledge, such guest-dependent, tunable CT interactions driving the folding of a discrete, flexible chromophore oligomer have rarely been investigated previously.

Results and discussion

Oligomer design and synthesis

The oligomer NDI-pentamer **1** was prepared in a multistep reaction involving coupling, protection, and deprotection steps. Pyridine has been considered a turn because of its easy functionalization protocol. It is anticipated to help the oligomer achieve a folded state by organizing NDI units in a sheet-like orientation for interlayer electronic interaction. It was functionalized with 2-ethylbutoxy to provide sufficient solubility to the oligomer. The interlinking alkyl chains that connect the pyridine and NDI units were strategically introduced to provide sufficient flexibility to the system, which may influence adaptable folding behaviour and could encapsulate guests within the sheets. In our initial design, the intention was to prepare all amide pentamers. However, challenges in the desymmetrisation of the NDI-monomer encouraged us to prepare a mixed ester and amide oligomer. Our studies revealed that the ester linkages are significantly stable and have allowed further functionalization.

The steps involved in the synthesis of **1** are given in Scheme 1. In brief, initially, the terminal block **7** was prepared starting from pyridine mono acid **2**. First, an amide coupling reaction with *N*-Boc-1,4-butanediamine, subsequent Boc deprotection, and imidization with naphthalene monoanhydride **5** provided **6**. It was further demethylated with LiI to get acid **7**. All these steps performed well with reasonably good yields. The NDI-*N*-Boc alcohol **9** was prepared starting from **8** in an imidization reaction. Subsequent coupling reaction with pyridine mono acid **2** and Boc-deprotection provided **11**, which was further reacted with **7** to obtain the NDI dimer block **12**. It was demethylated with LiI to obtain acid **13** quantitatively, establishing the stability of the other ester linkage under these conditions. Finally, an amide coupling reaction with the NDI diamine **14** provided the target oligomer **1** in a 35% yield, having five NDI units. It can be noted that the coupling reactions mostly worked better with hexafluorophosphate benzotriazole tetramethyl uronium (HBTU) over other coupling

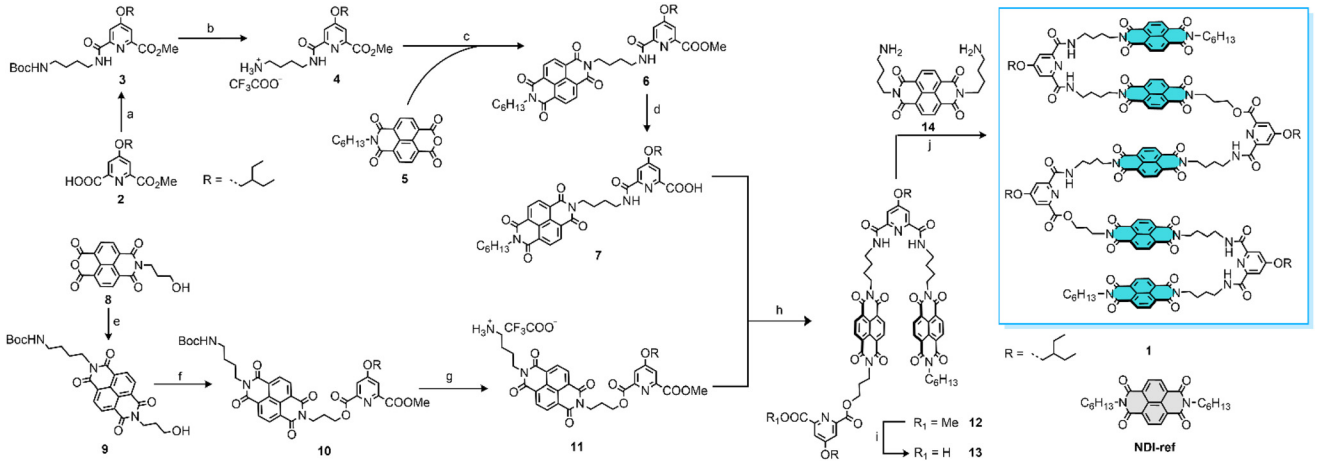

Scheme 1 The schematic flowchart of the synthesis of **1**. (a) (i) Oxalyl chloride, anhydrous DCM, 3 hours; (ii) *N*-Boc-1,4-butanediamine, THF, DIPEA, 2 hours, 85%. (b) TFA : DCM (1 : 2), 3 hours, quantitative. (c) DMF, DIPEA, 378 K, 15 hours, 58%. (d) LiI, anhydrous ethyl acetate, 351 K, 15 hours, 83%. (e) *N*-Boc-1,4-butanediamine, DMF, 373 K, 14 hours, 52%. (f) **2**, HBTU, DIPEA, DCM, 12 hours, 60%. (g) TFA : DCM (1 : 1), 3 hours, quantitative. (h) HBTU, DIPEA, DCM, 12 hours, 35%. (i) LiI, dry ethyl acetate, 351 K, 4 hours, quantitative. (j) EDC, HOBt, DIPEA, DMF, 12 hours, 35%.

reagents and generated fewer by-products, except for the final coupling, where 1-ethyl-3-(3-dimethylaminopropyl)carbodiimide (EDC) and hydroxybenzotriazole (HOBT) provided better yields. The detailed synthetic procedure is provided in the SI.

Characterization and electrochemical studies

Oligomer **1** was characterized by nuclear magnetic resonance (NMR), mass spectroscopy, and other analytical tools. The ^{1}H-NMR of **1** in $CDCl_3$ at 298 K shows a sharp set of signals (Fig. 2a and S1). The well-resolved signals in the aromatic region indicate the presence of the defined species. There are three different sets of NDI signals in the range of 8.7–8.5 ppm in a 2 : 2 : 1 ratio corresponding to the terminal, adjacent, and central NDI units with gradual upfield shifts. The splitting of the terminal NDI proton signals signifies that they are not chemically equivalent to each other. The weak splitting of the next NDI protons is an indication that all the protons are chemically equivalent and are not influenced much by the amide and ester linkages at both ends. All the protons of the central NDI give a singlet due to the symmetry. The separate and well-resolved signals for the three different types of NDI in the oligomer are indicative of the presence of an ordered structure (could be partially folded, *vide infra*), where the central NDI faces the highest ring current, thus more upfield shifted. The amide signals spread between 8.4 and 8.2 ppm in a 2 : 1 ratio corresponding to the three types of amide protons, with two amide signals merged (Fig. 2a and S2). The pyridine protons are observed within 7.8–7.6 ppm. The MALDI-TOF mass spectra also suggest the formation of oligomer **1** (Fig. S3). All these results collectively confirm the formation and purity of compound **1**.

To understand whether oligomer **1** has any temperature dependency, a variable temperature ^{1}H-NMR study was performed in $CDCl_3$ in a temperature range of 298–323 K, which indicates that the signals belonging to NDIs shifted slightly, while pyridine signals remained unaltered (Fig. 2b and S4). Additionally, the amide signals are upfield shifted and resolved. The well-distributed NDI signals and minute shift in temperature variation indicate that **1** is perhaps in the partially folded state, if not completely folded. The concentration-dependent NMR within the 0.5–5 mM range does not show any significant change either (Fig. S5), which confirms the absence of intermolecular aggregation within this concentration range. To understand the structure of **1**, we performed energy minimization of the oligomer using the Universal Force Field implemented in the Forcite module of Materials Studio. This reveals that the molecule is partially folded, where NDIs on both sides of the central NDI are paired with inter-NDI distances of ~3.6 Å (Fig. 2c and d). The overall length of the molecules is around 26.2 Å, which is close to the solvodynamic diameter (~29.8 Å) estimated from the ^{1}H-DOSY (Diffusion Ordered Spectroscopy) NMR experiment using the Stokes–Einstein equation (Fig. S6).

The absorption spectra of **1** (6×10^{-6} M) in DCM show typical bands similar to those of the NDI monomer (**NDI-ref**) with a characteristic vibronic feature for the S_0–S_1 transition with a maximum at around 381 nm ($A_{0\text{-}0}$), with vibronic progressions at 360 nm ($A_{0\text{-}1}$) and 343 nm ($A_{0\text{-}2}$) (Fig. 2e). The molar absorptivity (ε) of the $A_{0\text{-}0}$ band of **1** (1.48×10^5 M^{-1} cm^{-1}) is little less than five times that of **NDI-ref** (2.98×10^4 M^{-1} cm^{-1}). Presumably, the fact that the prevailing partially folded state of the oligomer in DCM, and some electronic interactions between NDI units, cannot be ruled out. The concentration-dependent UV-Vis studies of 3–50 μM solutions show a linear variation in absorbance, indicating insignificant molecular association within this concentration range (Fig. S7). Therefore, all other studies were performed at concentrations below 50 μM of **1**. The fluorescence spectroscopy revealed that the oligomer has a strong excimer-like emission at 500 nm along with typical monomer emission at 387 nm. It

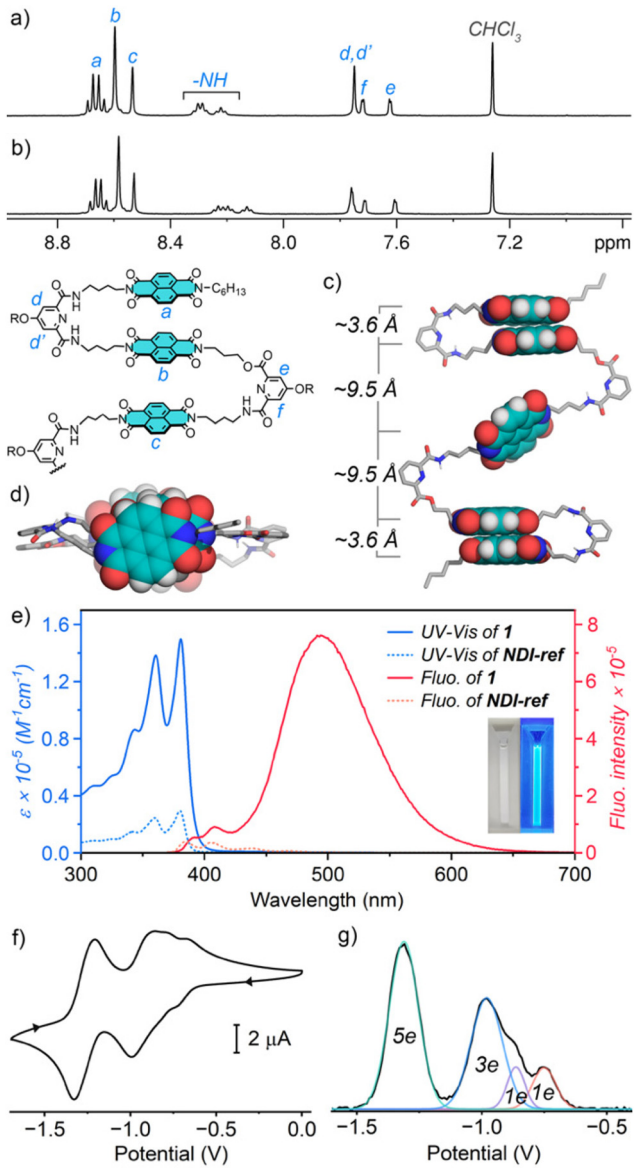

Fig. 2 Selected region of 400 MHz ^{1}H-NMR spectra of **1** (5 mM) in $CDCl_3$ with peak assignment at 298 K (a) and at 323 K (b). (c) Side and (d) top views of the energy-minimized models (Universal Force Field) of **1** with inter NDI distances showing the partially folded nature of the oligomer. Side chains are removed for clarity. (e) UV-Vis (6×10^{-6} M) and normalized fluorescence (λ_{ex} = 360 nm) spectra of **1** and **NDI-ref** in DCM at 298 K. The visual color of the solution of **1** under ambient and UV (365 nm) light. (f) Cyclic voltammogram (CV) of **1** (~0.2 mM) recorded using a glassy carbon working electrode and $Ag/AgNO_3$ as a reference electrode at a scan rate of 50 mV s^{-1} in Ar-purged anhydrous dichloromethane with 0.1 M Bu_4NPF_6 as a supporting electrolyte at 298 K. (g) Differential pulse voltammogram (DPV) in a 10 mV step pulse. All the potentials are given against Fc/Fc^+.

is known that the NDI derivatives have low monomeric fluorescence quantum yields and short fluorescence lifetimes due to the rapid deactivation of the S_1 state (in picoseconds) *via* intersystem crossing to a closely spaced triplet state.[68] An excimer-like emission, a rarely observed phenomenon due to the intermolecular stacking effect at the higher concentration, generally gives bright fluorescence.[69–71] Remarkably, oligomer **1** shows a bright excimer-like emission at as low as 5×10^{-6} M concentration with a quantum yield (QY) of 2.5%, indicative of the intramolecular phenomenon (Fig. 2e and S8). In contrast, **NDI-ref** does not show any excimer emission at low concentration. This further highlights the dynamic nature of the oligomer, where the NDI units organize in a partially folded state to provide intense excimer emission. The time-correlated single photon counting (TCSPC) measurements with excitation at 375 nm and monitoring emission at 500 nm provided a single exponential decay with a lifetime of 20 ns, confirming the excimer emission nature of the band (Fig. S9).

NDI derivatives are known for their exciting electrochemical properties, having two reversible one-electron reductions.[49–51,56] To understand the electrochemical properties of oligomer **1**, cyclic voltammetry (CV) was performed in DCM with Bu_4NPF_6 as a supporting electrolyte. This shows several reversible reduction waves, $E_{1/2}$ at −0.69 V, −0.92 V, and −1.27 V *vs.* Fc/Fc^+ (Fc: ferrocene) of varying intensities (Fig. 2f). To quantify the number of electrons involved in the reduction processes, differential pulse voltammetry (DPV) was performed at a 10 mV step pulse, and electron transfer was quantified against Fc/Fc^+ (Fig. 2g). The DPV showed a broad unresolved reduction in between −0.6 and −1.15 V, having a maximum at −0.98 V and humps at −0.86 V and −0.75 V. Another most intense signal was observed at −1.31 V. To quantify the number of electrons involved in each reduction process, we deconvoluted each band, which demonstrated that the broad signal (−0.6 V to −1.15 V) involves three clear reduction processes involving two one-electron reductions and then a three-electron reduction. The reduction at −1.31 V involves a five-electron process. These results are consistent with the total 10 electron reduction expected for oligomer **1**, comprising five NDI units, where each can undergo a two-electron reduction. The reduction processes between −0.6 V and −1.15 V are a result of the first reduction of the five NDI units involving one electron each. The reduction at −1.31 V originates from the second reduction of all NDI units, similar to **NDI-ref**, which has the first and second reductions at −0.91 V and −1.32 V (Fig. S10), respectively. Notably, even though the second reduction of all the NDI units happened at a similar potential, their first reduction did not occur simultaneously, but rather stepwise. This indicates that the first electron-accepting ability of all the NDIs was not the same. In particular, the relatively easier first reduction indicates that it has a higher electron affinity compared to the NDI monomer (**NDI-ref**). However, once the first reduction happens, subsequent reductions require higher potentials.

Solvent-dependent folding

The folding of the dye appended oligomers allows dye stacks, giving access to the exciton coupling between them.[37,39,72,73] Previous studies revealed that the folding of the dye oligomers can be significantly influenced by the solvent polarity.[40,44,45] Generally, in polar solvents, like DCM and chloroform, rylene

dyes tend to be solvated and have less tendency to be folded. However, nonpolar solvents can induce the folding that can be monitored by UV-Vis spectroscopy. The ratio of the vibronic absorptions ($A_{0\text{-}0}/A_{0\text{-}1}$) of the S_0–S_1 transition is often used to understand the extent of folding of the oligomers.[36,74–76] This method has been used to differentiate between the monomeric absorption and the presence of exciton coupling between them, influenced by the aggregation or folding. The $A_{0\text{-}0}/A_{0\text{-}1}$ ratio observed for **1** in DCM is 1.11, which is lower than that of **NDI-ref** ($A_{0\text{-}0}/A_{0\text{-}1}$ = 1.2) under similar conditions in DCM (Fig. S11), a solvent known for the excellent solvation properties of the rylene dyes. This lower $A_{0\text{-}0}/A_{0\text{-}1}$ value reaffirms that the oligomer is partially folded. However, this ratio for **NDI-ref** does not change in chloroform but has a higher value for **1** ($A_{0\text{-}0}/A_{0\text{-}1}$ = 1.16), an indication of the dominant unfolded state.

To induce the folding using a nonpolar solvent, MCH was added gradually (up to 60%) to a 6 μM chloroform solution of **1**, and the UV-Vis spectra were recorded subsequently. With the increase in the MCH proportion, the intensity of the $A_{0\text{-}1}$ band increased significantly compared to the $A_{0\text{-}0}$ band (Fig. 3a). The linear decrease of the $A_{0\text{-}0}/A_{0\text{-}1}$ ratio with respect to the proportion of MCH added clearly indicates significant electronic interaction between the NDI units as a result of the folding (Fig. 3c). Similar behaviour was observed when toluene was added to the solution of **1** in $CHCl_3$ (Fig. 3b). Interestingly, the change was more prominent, where the $A_{0\text{-}0}/A_{0\text{-}1}$ ratio reduced to 1.01 compared to 1.05 in MCH from 1.16 in $CHCl_3$. Additionally, the band became broader with significant absorption at 400 nm compared to the MCH scenario. This is due to the charge transfer interaction between the NDI units and toluene, in accordance with the previous observations of NDI monomers.[77] Similar trends were observed for other aromatic hydrocarbons such as *p*-xylene and mesitylene (Fig. S12 and S13). These solvent-dependent changes in the absorption spectra at low concentrations can be unambiguously attributed to the intramolecular folding, as no spectral changes were observed when the concentration was increased to 10^{-5} M in chloroform (Fig. S7). Moreover, the $A_{0\text{-}0}/A_{0\text{-}1}$ ratio remained nearly constant when the concentration was varied from 1.5 × 10^{-6} M to 25 × 10^{-6} M with 50% MCH and toluene addition in chloroform, further ascertaining the solely intramolecular folding behaviour (Fig. 3d).

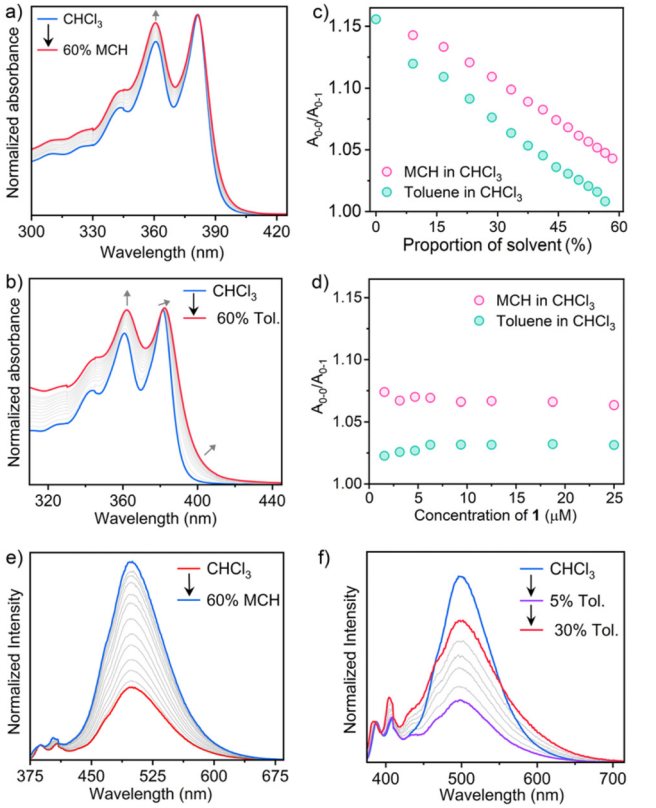

Fig. 3 UV-Vis spectral changes upon gradual addition of 60% MCH (a) and toluene (b) in a 6 μM solution of **1** in chloroform at 298 K. Both results are plotted with normalization of absorbance at 381 nm ($A_{0\text{-}0}$) to see the changes at 361 nm ($A_{0\text{-}1}$), which clearly intensified on MCH and toluene addition. (c) Plots showing linear variations of the $A_{0\text{-}0}/A_{0\text{-}1}$ ratio with increasing proportions of MCH and toluene, where the latter has a more pronounced effect than the former. (d) Variation of the $A_{0\text{-}0}/A_{0\text{-}1}$ ratio after the addition of 50% MCH or toluene at different concentrations of **1** in $CHCl_3$. Nearly unchanged variation clearly signifies an intramolecular folding process that intensifies the $A_{0\text{-}1}$ band. (e) Change in excimer emission intensity after the gradual addition of MCH (up to 60%) in a 6 μM solution of **1** in $CHCl_3$. The fluorescence was normalized at 387 nm (monomeric emission). (f) Change in the fluorescence of **1** upon addition of toluene. Quenching of fluorescence was observed after the addition of 5% toluene. Then further addition of toluene results in CT emission. The emission was normalized at 387 nm. The samples were excited at 360 nm.

Folding-induced emission properties

To investigate the effect of solvent addition on the emission properties, the fluorescence was measured with varying proportions of MCH and toluene in chloroform. Interestingly, with increasing MCH proportion, the intensity of the excimer fluorescence band was significantly enhanced after addition of 60% MCH (Fig. 3e). This is evident from the enhancement of the QY to 5.9% from 2.5% in chloroform. This further establishes solvent-dependent reinforced folding of the oligomer that brings NDI units closer, facilitating excimer formation. In contrast, the effect of toluene addition on fluorescence is more complex. Initially, the gradual addition of 5% toluene to the solution of **1** in chloroform (6 × 10^{-6} M) resulted in quenching of the excimer fluorescence (Fig. 3f). Then, upon further addition of toluene (up to 30%), a broad fluorescence emission having a maximum at 500 nm, the same wavelength as the excimer emission, appeared before being saturated in further increments of toluene proportion. The quenching of the excimer fluorescence is perhaps due to facile charge transfer (CT) between toluene molecules and NDI units of the oligomer. Consequently, it provides a broad CT emission band with an increasing toluene proportion. The overall QY reduced to 1.1% after addition of 30% toluene. This observation is consistent with the UV-Vis studies, where the addition of toluene yielded a CT absorption at around 400 nm (Fig. 3b). To further

ascertain it, we performed fluorescence titrations with *p*-xylene and mesitylene, which provide a similar behaviour and have CT emissions at 536 nm and 540 nm, respectively (Fig. S14). Remarkably, this system exhibits a multifaceted fluorescence property, a rare phenomenon, depending on the solvent. To understand the lifetimes of the different emission processes, we performed TCSPC measurements by exciting the sample in $CHCl_3$ at 375 nm and monitoring at 500 nm before and after the addition of MCH. The fluorescence decays were fitted with a single exponential to estimate the lifetimes of these emission processes to be 20 ns and 19.8 ns, respectively. The similar lifetimes of these bands after the addition of MCH in a $CHCl_3$ solution of **1** indicate identical emission processes. However, after the addition of toluene, the band at 500 nm has a relatively faster decay with a lifetime of 0.25 ns, confirming our anticipation of the formation of the CT emission band (Fig. S15). The emission bands originating from the interaction of *p*-xylene and mesitylene also have similar lifetimes of 0.51 ns and 0.38 ns, respectively (Fig. S16), further establishing their CT nature.

Guest-dependent folding and tunable charge-transfer

Motivated by the CT phenomenon observed with toluene, *p*-xylene, and mesitylene, we anticipated that polyaromatic donors may interact with **1** by leveraging donor–acceptor π–π interactions with the NDI units. Such interactions may also give rise to the CT phenomenon in the visible range, providing interesting photophysical properties fundamental for optoelectronics. Moreover, they might assist the folding of the oligomer by intercalating within the NDI sheets and creating a long-range donor–acceptor stack. To explore it, first, we titrated **1** with perylene (**Pe**), in $CHCl_3$ at 298 K. A gradual rise of the broad characteristic CT-band was observed at 600 nm, which got saturated after the addition of nearly 4 equivalents of the **Pe** (Fig. 4a), corroborating the four cleft-like cavities available in the oligomer. This result emphasizes that the **Pe** molecules favor the folded conformer of **1** and stabilize it by D–A interaction. Notably, during this process, the colorless solution of **1** turned dark green, signifying its complexation. The variable temperature UV-Vis studies of the mixture indicate that the CT-complex becomes dominated with an intensified CT-band at 278 K (Fig. 4b). However, the intensity reduces at higher temperatures, forcing the disassembly of the complex, a characteristic feature of the CT-complexes.

Encouraged by this finding, we tested a few other polyaromatic guests (Fig. 1c), such as naphthalene (**Np**), anthracene (**An**), carbazole (**Cz**), phenanthrene (**Pn**), triphenylene (**Tp**), and pyrene (**Py**), with varying size and donor ability to explore whether they provide tunable CT-behaviour (Fig. S17–S22). Titrations with these guests further demonstrate their ability to interact with **1**, but interestingly, they have different CT absorption bands (λ_{CT}, Table 1) ranging from 450 nm for **Np** to 600 nm for **Pe** with tunable visual color changes of the solution with guest addition (Fig. 4c). Astonishingly, their absorption can be tuned within the whole visible region depending on the guests (Fig. 4c inset). Such a strong CT interaction in chloroform is notable, where both **1** and the guests tend to be solvated and possess low to medium association constants. The discrete folded structure of the oligomer perhaps allows a relatively stronger interaction between them that results in a long-range D–A order. The CT absorption intensity also varies depending on the guests. This could be related to the electronic complementarity between **1** and the guests, while the π surface of the guests may also contribute to the dispersive interaction. To ascertain whether the cleft-like cavities between the NDI sheets are responsible for such efficient CT complexation, we performed UV-Vis titration of **NDI-ref** with **Pe**. We observed the appearance of a weak CT band even after the addition of a large excess of **Pe** (6 equivalents; Fig. S23). This further indicates their influence in the folding process of **1** and the role of the cavities in guest intercalation.

To quantify the strength of CT-complexation, we attempted to estimate the association constants (K_a) by fitting the change in absorbance of the CT band with the equivalent of the guest added using a 1 : 1 binding model (Fig. S24–S26).[78] The findings summarized in Table 1 show that perylene has the highest K_a with 291.41 M^{-1} compared to other polyaromatic donors. This trend primarily follows their electron-donating abilities, since CT is related to an intermolecular interaction between the highest occupied molecular orbital (HOMO) of the polyaromatic guests and the lowest unoccupied molecular orbital (LUMO) of **1**. However, **Tp** displays a higher K_a than

Table 1 Estimated association constants (K_a), molar absorptivities (ε_{CT}), and changes in the Gibbs free energy ($\Delta G°$) of CT-complexation obtained from the change in the absorbance of the CT-band with the concentration of the host using 1 : 1 and 1 : 4 models

	NDI-ref		**1**					
	1 : 1 model		1 : 1 model			1 : 4 model		
Guests	K_a [a] (M^{-1})	$-\Delta G°_{298}$ [c] (kJ mol^{-1})	λ_{CT} (nm)	K_a [a] (M^{-1})	$-\Delta G°_{298}$ [c] (kJ mol^{-1})	K_a [b] (M^{-1})	ε_{CT} [b] (M^{-1} cm^{-1})	$-\Delta G°_{298}$ [c] (kJ mol^{-1})
Pe	31.82	8.57	600	291.41	14.06	14.04	945.85	6.54
An	—	—	526	92.77	11.22	10.76	182.02	5.88
Cz	—	—	506	75.27	10.71	8.82	458.22	5.39
Py	—	—	513	93.26	11.24	7.88	555.85	5.11
Tp	—	—	444	103.21	11.49	7.18	1170.67	4.88
Pn	—	—	443	67.84	10.45	6.19	566.21	4.51

[a] K_a was estimated using a 1 : 1 binding model. [b] K_a and ε_{CT} were calculated using eqn (1). [c] $\Delta G° = -RT \ln K_a$ at T = 298 K.

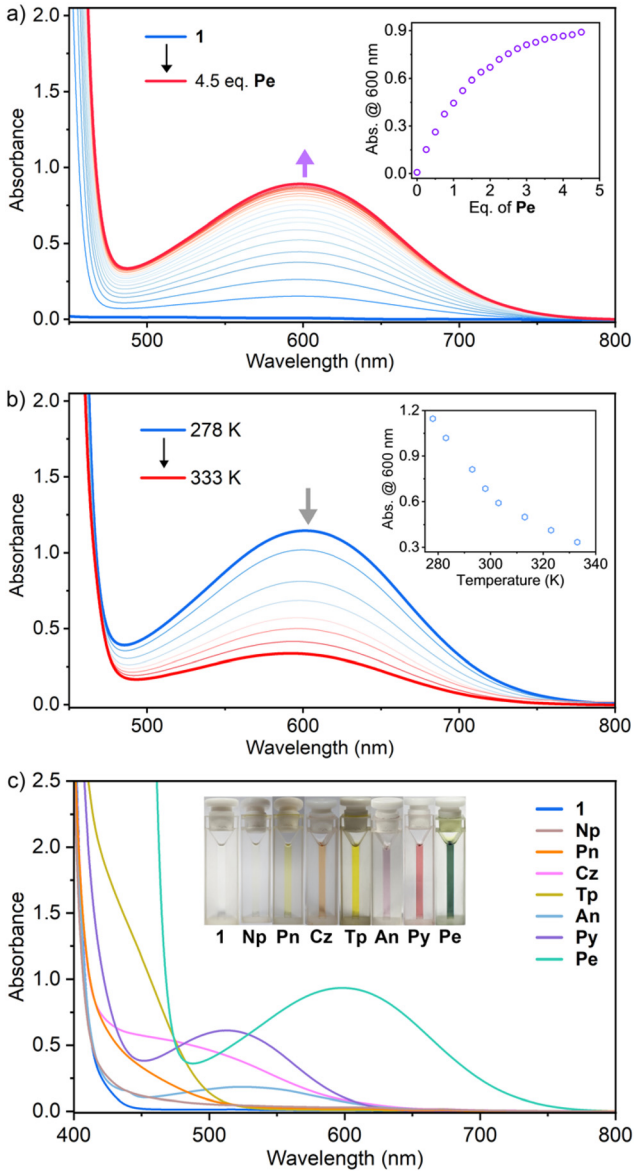

Fig. 4 (a) Changes in the UV-Vis absorption spectra of **1** (3 mM) upon titration with perylene (**Pe**) in chloroform at 298 K. Blue lines: spectra before titration; red lines: spectra after 4.5 equivalents of **Pe** were added. The arrow indicates the appearance of a strong charge transfer (CT) band. Inset: variation of absorbance at 600 nm with respect to increasing **Pe** equivalence. (b) Temperature dependency of the CT band within the temperature range of 278–323 K. Inset: variation of absorbance at 600 nm with temperature. (c) Guest-dependent variation of the charge transfer band and consequent visible color change (inset).

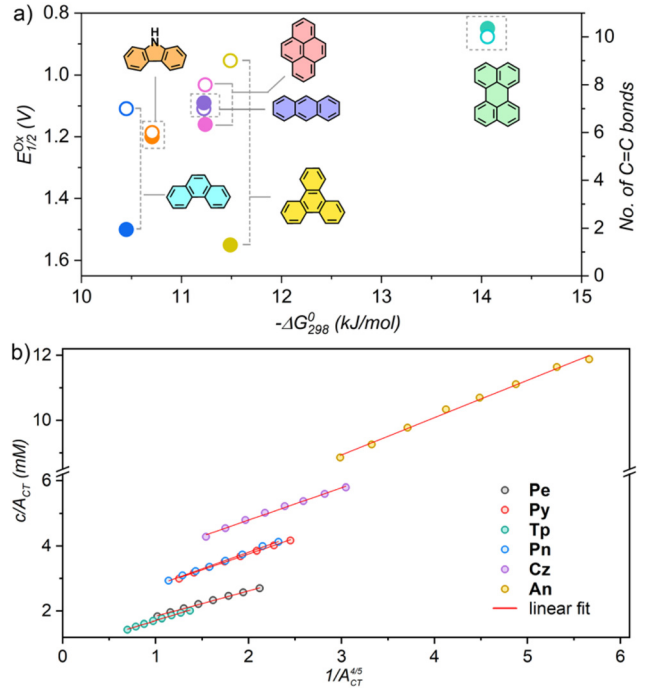

Fig. 5 (a) The variation of free energy of stabilization $(-\Delta G^{\circ}_{298})$ obtained from the 1 : 1 binding model (Table 1) with the $E^{Ox}_{1/2}$ (filled circles) and the number of C=C bonds (empty circles) on guests. The lower $E^{Ox}_{1/2}$ represents better electronic complementarity to CT complexation. Large π-surface (higher C=C bonds) contributes to the dispersive interaction. (b) The variation of c/A_{CT} *vs.* $1/A^{4/5}_{CT}$ when the concentration (*c*) of **1** was varied, maintaining a constant 4 equivalents of guests, and the absorbance (A_{CT}) of the CT band was measured. The K_a and ε_{CT} values were estimated from the slope and intercept of the linear fit of each variation.

expected from the relative HOMO energy alone (Fig. S45). We presume that the existence of some dispersion interaction is involved, where the large π-surface area (greater number of C=C bonds) of the guests contributes to K_a.[79] To examine this further, we plotted the free energy of stabilization $(-\Delta G^{\circ}_{298})$ against the oxidation potential $(E^{Ox}_{1/2})$ and the number of C=C bonds in each guest (Fig. 5a). The $E^{Ox}_{1/2}$ is directly related to the HOMO of the guests; the higher HOMO energy reflects lower $E^{Ox}_{1/2}$, thus making the guest a better donor. The trend shows that $-\Delta G^{\circ}_{298}$ increases with the lower $E^{Ox}_{1/2}$ and an increasing number of C=C bonds of the guests, following the order **Pn** < **Cz** < **Py** ≈ **An** ≈ **Tp** < **Pe** (Fig. 5a). As expected, **Pe** displays the highest $-\Delta G^{\circ}_{298}$ owing to its lowest $E^{Ox}_{1/2}$ (0.85 V) and maximum C=C bonds. **Py** and **An** exhibit similar values; the slightly higher $E^{Ox}_{1/2}$ of **Py** (1.16 V *vs.* 1.09 V for **An**) is compensated for by the one extra C=C bond present in it. The unusually higher $-\Delta G^{\circ}_{298}$ value for **Tp** is dominated by its greater C=C bonds, despite its high $E^{Ox}_{1/2}$ (1.55 V). A similar effect is observed for **Pn**, whereas **Cz** follows the expected trend. Overall, the extent of host–guest complexation is a result of complementary electronic effects as well as π-surface area.

Since **1** has four cleft-like cavities that can accommodate four guests and, as reflected by the UV-Vis titration in some cases, the saturation of CT absorbance is observed after the addition of four equivalents of guest, we considered a 1 : 4 model as well, modifying the previously reported 1 : 1 model by Stoddart and co-workers (see the SI for details).[80] This assumes that the appearance of the absorbance of the CT-band is solely a result of the association of the host and the guests and the formation of the 1 : 4 complex. Here, the absorbance of the CT-band (A_{CT}) was monitored from UV-Vis spectra as a function of host (**1**) concentration, while 4

equivalents of guest were added every time (Fig. S27–S29). The K_a and molar extinction coefficient (ε_{CT}) of the CT complex were estimated from the slope and intercept of the c/A_{CT} *vs.* $1/A_{CT}^{4/5}$ linear plot (Fig. 5b) using the following equation.

$$\frac{c}{A_{CT}} = \frac{1}{\sqrt[5]{256K_a\varepsilon_{CT}l}} \cdot \frac{1}{A_{CT}^{4/5}} + \frac{1}{\varepsilon_{CT}l} \quad (1)$$

where c and l represent the initial concentration of the host and the optical path length, respectively. The linear variation of c/A_{CT} *vs.* $1/A_{CT}^{4/5}$ is also an indication of the intramolecular CT complexation between **1** and polyaromatic guests rather than an intermolecular phenomenon. The estimated K_a values are summarized in Table 1. It can be noted that the K_a values obtained from the previous method are much higher than those obtained from the subsequent method. This is because the K_a estimated in the second method is the average association constant in the case of stepwise complexation of four guests in **1**. The estimation of individual association constants in every binding and the understanding of the presence of any cooperativity in the binding process cannot be performed due to the complexity of the process. However, the first and second guest binding are expected to be stronger than the subsequent binding simply because each guest binding to the host makes it less electron-deficient than its native state. Nevertheless, this method gives an overall understanding of the difference in the CT complex formation with various guests.

Considering that all the guests have different CT absorptions and **1** has four cleft-like cavities, we wanted to explore the possibility of double CT interaction by adding two different guests to **1**. Double CT interaction allows obtaining an exciting functional system that can absorb broad visible light and may enable efficient charge separation. For this purpose, first, we titrated **1** with two equivalents of **Tp**, followed by another two equivalents of **Py**. Initially, during the addition of **Tp**, we observed the appearance of a CT band at 444 nm, and then, upon subsequent addition of **Py**, another CT band appeared, having a maximum at 513 nm (Fig. 6a). It covers a broad absorption between 430 and 600 nm, consisting of two CT bands, a signature of NDI–Tp and NDI–Py CT interactions. A similar experiment was conducted by simultaneously adding **Py** and **Pe**, covering the absorption range from 480 to 750 nm, even though the CT band due to the NDI–Py interaction was to some extent shadowed by the absorption of unbound **Pe** (Fig. 6b). Although the exact arrangement of the guests in the cavities is not clear, the demonstration of multiple guest-dependent broad CT absorption in the visible light could be promising for photoinduced charge separation.

To further probe the interaction between **1** and the polyaromatic guests, we performed ^{1}H-NMR titrations in $CDCl_3$ at 298 K. Fig. 7a–g shows the representative ^{1}H-NMR titration spectra upon gradual addition of **Pe** solution in **1**, while details about titrations with other guests are provided in the SI (Fig. S30–S35). After the addition of **Pe** (5 eq.), the signals from NDI units are upfield shifted, with the changes being most prominent in the case of the central NDI signal, which exhibits

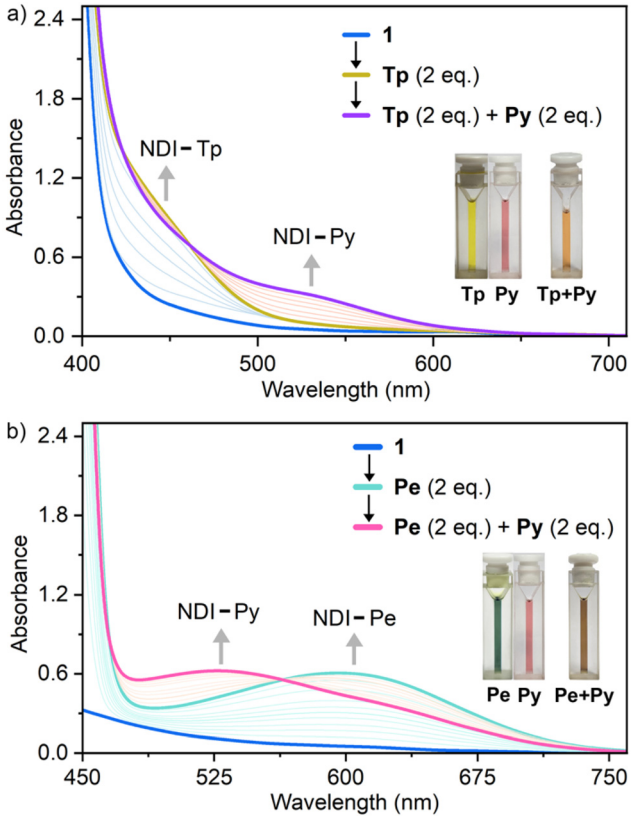

Fig. 6 Changes in the UV-Vis absorption spectra of **1** (3 mM) upon subsequent addition of (a) **Tp** (2 eq.) and **Py** (2 eq.) and (b) **Pe** (2 eq.) and **Py** (2 eq.) in chloroform at 298 K. The arrows indicate the CT bands corresponding to NDI–Tp, NDI–Py and NDI–Pe interactions. Inset: distinct visual color changes of the solution after the addition of only **Tp**, **Py**, and **Pe**, and the combination of **Tp** + **Py** or **Pe** + **Py** to the solution of **1**.

a ~1.1 ppm shift, compared to a ~0.7 ppm shift for signals from the other NDIs (Fig. 7a–f). Additionally, the signals from **Pe** are also shifted upfield compared to free **Pe** signals (Fig. 7g). This is consistent with the fact that the intercalation of the **Pe** into the clefts of folded **1** enhances ring current, resulting in such an upfield shift of the signals of both the host and guest. It is interesting to note that, quite expectedly, the signals from pyridine units remained mostly unaltered during the titration process, signifying that the host–guest interaction does not change their environment. This also indicates that the process is a molecular phenomenon and does not involve any intermolecular assembly induced by the guest. Similar changes are observed for other guests; however, the extents of changes remain different, and consistent with the electron-donating ability of the guests. To understand the temperature dependency of the CT complex, we performed VT ^{1}H-NMR in $CDCl_3$ within 298–323 K. It is evident that with increasing temperature, the signals of NDI protons of **1** as well as **Pe** started to shift downfield, indicating the decomplexation (Fig. 7h and i and Fig. S36–S42) process. This is in accordance with the VT studies using the UV-Vis method.

To determine whether the CT complexation is an intramolecular phenomenon or involves intermolecular assembly,

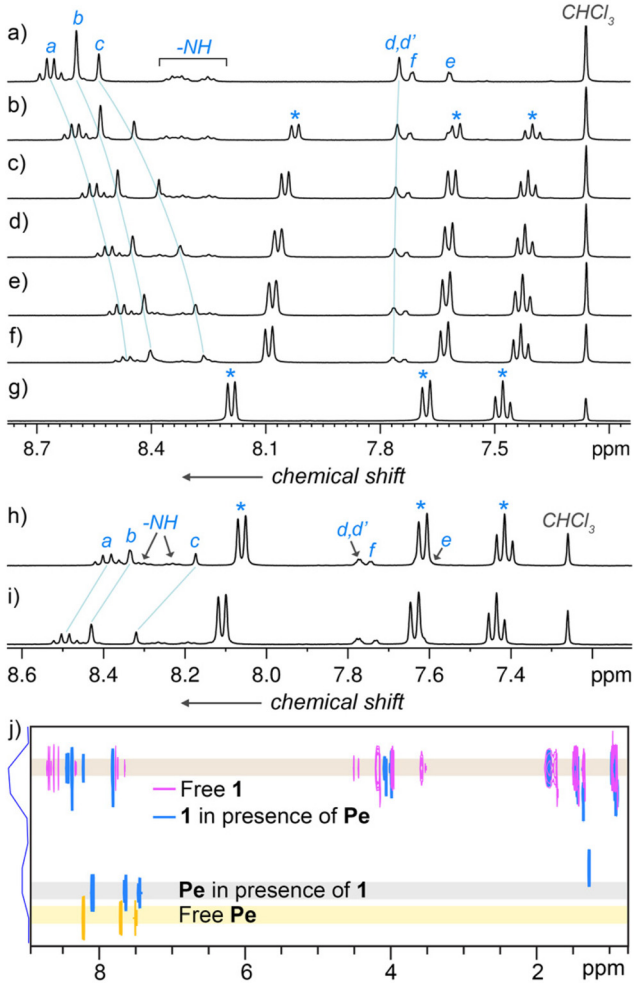

Fig. 7 (a) Partial 400 MHz ^{1}H-NMR spectra of **1** (3 mM) in $CDCl_3$ and upon addition of 1 (b), 2 (c), 3 (d), 4 (e), and 5 equivalents (f) of **Pe** (15 mM in $CDCl_3$) at 298 K. (g) The ^{1}H-NMR spectrum of **Pe** (10 mM) in $CDCl_3$ is given for comparison. The cyan lines indicate the changes in the signals of **1** upon the addition of the guest. The asterisk (*) represents signals appearing from **Pe**. (h and i) Variable temperature ^{1}H-NMR of [**1** + **Pe**] (at a constant 3 mM concentration of **1**) at 298 K and 323 K, respectively, in $CDCl_3$. (j) Overlaid DOSY-NMR spectra of [**1** + **Pe**] (blue), free **1** (magenta), and free **Pe** (orange contour). The brown shade represents diffusion of **1** with and without **Pe**. The identical diffusion rate indicates no intermolecular association of **1** in the presence of **Pe**. The grey shade represents the diffusion of **Pe** in the presence of **1**. It is distinctly different from the diffusion rate of free **Pe** highlighted in a yellow shade.

we performed ^{1}H-DOSY NMR. Fig. 7j clearly shows that after the addition of five equivalents of **Pe** in **1** the diffusion coefficient is comparable to that of free **1**. The diffusion coefficient of the **Pe** in the mixture is different from that of **Pe** when measured separately. The diffusion of **Pe** does not follow along the host due to the rapid exchange between the bound and free **Pe** in the medium. The overall studies indicate that the complexation is an intramolecular phenomenon rather than an intermolecular assembly assisted by **Pe**.

Attempts to elucidate the structures of the CT complexes by X-ray crystallography were unsuccessful, as multiple crystallization efforts failed to yield suitable single crystals. Nevertheless, we carried out energy minimization of the guest-intercalated oligomer using the Universal Force Field implemented in the Forcite module of Materials Studio. As expected, the optimized structures reveal an ordered, long-range alternate D–A stack. Representative models of the CT complexes of **1** with **Pe** and **Py** are given in Fig. 8, while models for other CT complexes are given in the SI (Fig. S43 and S44). In both cases, the guests are occupied within the clefts of **1** and are stabilized by CT interactions with adjacent NDI units. The NDI–guest distances are approximately 3.5 Å, consistent with close contact and strong CT interaction. Notably, the overall length of the CT complexes (~27.4 Å) is nearly identical to that of the uncomplexed oligomer **1** (~26.2 Å). This similarity is further supported by DOSY NMR measurements, which show insignificant change in diffusion coefficients upon addition of five equivalents of guest molecules. The estimated solvodynamic diameter using the Stokes–Einstein equation is 31.1 Å, which is in very good agreement with the theoretical **Pe** intercalated molecular length of **1** (27.4 Å) and close to the estimated diameter of the free oligomer (29.8 Å).

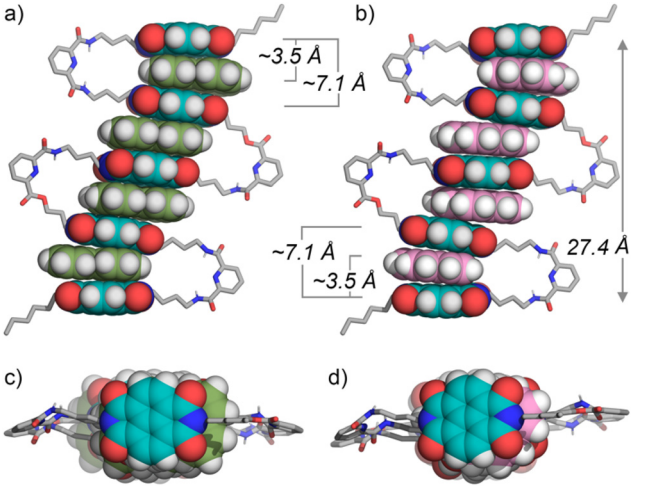

Fig. 8 (a and b) Side views of the energy-minimized models obtained using the Universal Force Field implemented in the Forcite module of Materials Studio for **Pe** and **Py** intercalated CT complexes of **1**, respectively, with distances between NDI and **Pe** or **Py**. (c and d) Their corresponding top views. The arrangement shows a long-range D–A order. Some hydrogen atoms and solubilizing side chains are omitted for clarity.

Conclusions

In conclusion, we have prepared a covalently linked, electroactive, conformationally flexible NDI-pentamer, **1**, through an iterative synthetic process that exhibits 10-electron reduction and a solvent-dependent folding behavior. While it remains partially folded in DCM and chloroform, as evidenced by strong excimer emission even at submicromolar concentrations, the addition of nonpolar solvents such as MCH or

toluene promotes further folding. This leads to enhanced excimer emission in MCH, whereas toluene quenches the excimer emission and provides a distinct weak CT emission. Additionally, folding has also been induced by polyaromatic donors such as perylene, pyrene, anthracene, triphenylene, *etc*., that intercalate between NDI layers through D–A interactions. The resulting CT responses are tunable and depend primarily on the electron-donating strength of the guests, while there is some contribution of dispersive interaction. Furthermore, sequential addition of two different donors provided dual CT bands leading to broad visible light absorption. The host–guest interactions have been investigated by extensive UV-Vis and NMR studies. Such guest-dependent folding of a flexible multidecker NDI system is unprecedented and offers new insight into conformational control and charge transfer within π-stacked materials. The resulting formation of long-range D–A arrays highlights the potential of such systems for light harvesting and charge-transport applications in organic electronics. Further studies along these directions will be reported in due course.

Author contributions

B. G. conceived the project. D. D. prepared the oligomer and conducted the experiments. D. T. helped in the electrochemical and spectroscopic studies and performed the computational investigations. B. G. supervised the research, performed the analysis, and wrote the manuscript. All the authors contributed to the preparation of the final manuscript.

Conflicts of interest

There are no conflicts to declare.

Data availability

The data supporting this article have been included as part of the supplementary information (SI). Supplementary information is available. See DOI: **https://doi.org/10.1039/d6qo00055j**.

Acknowledgements

We thank Shiv Nadar Institution of Eminence (SNIoE), Delhi NCR, for financial support and acknowledge the DST-FIST scheme (SR/FST/CS-I/2017/13(C)) for the MALDI facility.

References

1 S. S. Babu, V. K. Praveen and A. Ajayaghosh, Functional π-Gelators and Their Applications, *Chem. Rev.*, 2014, **114**, 1973–2129.
2 D. Bialas, E. Kirchner, M. I. S. Röhr and F. Würthner, Perspectives in Dye Chemistry: A Rational Approach toward Functional Materials by Understanding the Aggregate State, *J. Am. Chem. Soc.*, 2021, **143**, 4500–4518.
3 Z. Chen, A. Lohr, C. R. Saha-Möller and F. Würthner, Self-assembled π-stacks of functional dyes in solution: structural and thermodynamic features, *Chem. Soc. Rev.*, 2009, **38**, 564–584.
4 S. J. George, R. de Bruijn, Ž. Tomović, B. Van Averbeke, D. Beljonne, R. Lazzaroni, A. P. H. J. Schenning and E. W. Meijer, Asymmetric Noncovalent Synthesis of Self-Assembled One-Dimensional Stacks by a Chiral Supramolecular Auxiliary Approach, *J. Am. Chem. Soc.*, 2012, **134**, 17789–17796.
5 M. Hecht and F. Würthner, Supramolecularly Engineered J-Aggregates Based on Perylene Bisimide Dyes, *Acc. Chem. Res.*, 2021, **54**, 642–653.
6 J. K. Klosterman, Y. Yamauchi and M. Fujita, Engineering discrete stacks of aromatic molecules, *Chem. Soc. Rev.*, 2009, **38**, 1714–1725.
7 C. Röger, Y. Miloslavina, D. Brunner, A. R. Holzwarth and F. Würthner, Self-Assembled Zinc Chlorin Rod Antennae Powered by Peripheral Light-Harvesting Chromophores, *J. Am. Chem. Soc.*, 2008, **130**, 5929–5939.
8 F. Würthner, T. E. Kaiser and C. R. Saha-Möller, J-Aggregates: From Serendipitous Discovery to Supramolecular Engineering of Functional Dye Materials, *Angew. Chem., Int. Ed.*, 2011, **50**, 3376–3410.
9 F. Würthner, C. R. Saha-Möller, B. Fimmel, S. Ogi, P. Leowanawat and D. Schmidt, Perylene Bisimide Dye Assemblies as Archetype Functional Supramolecular Materials, *Chem. Rev.*, 2016, **116**, 962–1052.
10 L. Ernst, H. Song, D. Kim and F. Würthner, Photoinduced stepwise charge hopping in π-stacked perylene bisimide donor–bridge–acceptor arrays, *Nat. Chem.*, 2025, **17**, 767–776.
11 P. D. Frischmann, K. Mahata and F. Würthner, Powering the future of molecular artificial photosynthesis with light-harvesting metallosupramolecular dye assemblies, *Chem. Soc. Rev.*, 2013, **42**, 1847–1870.
12 Y. Han, X. Zhang, Z. Ge, Z. Gao, R. Liao and F. Wang, A bioinspired sequential energy transfer system constructed via supramolecular copolymerization, *Nat. Commun.*, 2022, **13**, 3546.
13 C. Lin, T. Kim, J. D. Schultz, R. M. Young and M. R. Wasielewski, Accelerating symmetry-breaking charge separation in a perylenediimide trimer through a vibronically coherent dimer intermediate, *Nat. Chem.*, 2022, **14**, 786–793.
14 B. Mu, X. Hao, X. Luo, Z. Yang, H. Lu and W. Tian, Bioinspired polymeric supramolecular columns as efficient yet controllable artificial light-harvesting platform, *Nat. Commun.*, 2024, **15**, 903.
15 Y. Zhang, Y. Han, S. Yuan, R. Liao, J. Chen and F. Wang, Simultaneous chirality and energy transfer of donor–acceptor chromophores via bio-inspired supramolecular light-harvesting, *Nat. Commun.*, 2025, **16**, 5862.

16 Q. Song, S. Goia, J. Yang, S. C. L. Hall, M. Staniforth, V. G. Stavros and S. Perrier, Efficient Artificial Light-Harvesting System Based on Supramolecular Peptide Nanotubes in Water, *J. Am. Chem. Soc.*, 2021, **143**, 382–389.
17 M. Hao, G. Sun, M. Zuo, Z. Xu, Y. Chen, X.-Y. Hu and L. Wang, Supramolecular Artificial Light-Harvesting System with Two-Step Sequential Energy Transfer for Photochemical Catalysis, *Angew. Chem., Int. Ed.*, 2020, **59**, 10095–10100.
18 Q. Zou, K. Liu, M. Abbas and X. Yan, Peptide-Modulated Self-Assembly of Chromophores toward Biomimetic Light-Harvesting Nanoarchitectonics, *Adv. Mater.*, 2016, **28**, 1031–1043.
19 K. V. Rao, K. K. R. Datta, M. Eswaramoorthy and S. J. George, Light-Harvesting Hybrid Hydrogels: Energy-Transfer-Induced Amplified Fluorescence in Noncovalently Assembled Chromophore–Organoclay Composites, *Angew. Chem., Int. Ed.*, 2011, **50**, 1179–1184.
20 M. R. Wasielewski, Self-Assembly Strategies for Integrating Light Harvesting and Charge Separation in Artificial Photosynthetic Systems, *Acc. Chem. Res.*, 2009, **42**, 1910–1921.
21 A. Ajayaghosh, V. K. Praveen, C. Vijayakumar and S. J. George, Molecular Wire Encapsulated into π Organogels: Efficient Supramolecular Light-Harvesting Antennae with Color-Tunable Emission, *Angew. Chem., Int. Ed.*, 2007, **46**, 6260–6265.
22 C. Röger, M. G. Müller, M. Lysetska, Y. Miloslavina, A. R. Holzwarth and F. Würthner, Efficient Energy Transfer from Peripheral Chromophores to the Self-Assembled Zinc Chlorin Rod Antenna: A Bioinspired Light-Harvesting System to Bridge the "Green Gap", *J. Am. Chem. Soc.*, 2006, **128**, 6542–6543.
23 F. Koch, M. Stolte, A. Zitzler-Kunkel, D. Bialas, A. Steinbacher, T. Brixner and F. Würthner, Unraveling the structure and exciton coupling for multichromophoric merocyanine dye molecules, *Phys. Chem. Chem. Phys.*, 2017, **19**, 6368–6378.
24 C. Yao, B. Gole, A. T. Bui, B. Kauffmann, I. Huc, N. D. McClenaghan and Y. Ferrand, Photon-gated foldaxane assembly/disassembly, *Chem. Commun.*, 2024, **60**, 8415–8418.
25 J. Atcher, P. Mateus, B. Kauffmann, F. Rosu, V. Maurizot and I. Huc, Large-Amplitude Conformational Changes in Self-Assembled Multi-Stranded Aromatic Sheets, *Angew. Chem., Int. Ed.*, 2021, **60**, 2574–2577.
26 B. Gole, B. Kauffmann, V. Maurizot, I. Huc and Y. Ferrand, Light-Controlled Conformational Switch of an Aromatic Oligoamide Foldamer, *Angew. Chem., Int. Ed.*, 2019, **58**, 8063–8067.
27 J. Atcher, A. Nagai, P. Mayer, V. Maurizot, A. Tanatani and I. Huc, Aromatic β-sheet foldamers based on tertiary squaramides, *Chem. Commun.*, 2019, **55**, 10392–10395.
28 A. Lamouroux, L. Sebaoun, B. Wicher, B. Kauffmann, Y. Ferrand, V. Maurizot and I. Huc, Controlling Dipole Orientation through Curvature: Aromatic Foldamer Bent β-Sheets and Helix–Sheet–Helix Architectures, *J. Am. Chem. Soc.*, 2017, **139**, 14668–14675.
29 L. Sebaoun, V. Maurizot, T. Granier, B. Kauffmann and I. Huc, Aromatic Oligoamide β-Sheet Foldamers, *J. Am. Chem. Soc.*, 2014, **136**, 2168–2174.
30 P. Prabhakaran, V. G. Puranik, J. N. Chandran, P. R. Rajamohanan, H.-J. Hofmann and G. J. Sanjayan, Novel foldamer structural architecture from cofacial aromatic building blocks, *Chem. Commun.*, 2009, 3446–3448, DOI: 10.1039/B822113H.
31 B. Gole, B. Kauffmann, A. Tron, V. Maurizot, N. McClenaghan, I. Huc and Y. Ferrand, Selective and Cooperative Photocycloadditions within Multistranded Aromatic Sheets, *J. Am. Chem. Soc.*, 2022, **144**, 6894–6906.
32 R. Rabban, D. Das, D. Talukdar and B. Gole, A multi-stack porphyrin oligomer with three cleft-like cavities for efficient guest encapsulations, *Chem. Commun.*, 2025, **61**, 8071–8074.
33 B. Teichmann, B. Liu, M. Hirsch, R. K. Dubey and F. Würthner, Sequential Synthesis and Secondary Structure Analysis of Two Classes of Perylene Bisimide Oligomers, *Org. Lett.*, 2024, **26**, 5544–5548.
34 B. Liu, Y. Vonhausen, A. Schulz, C. Höbartner and F. Würthner, Peptide Backbone Directed Self-Assembly of Merocyanine Oligomers into Duplex Structures, *Angew. Chem., Int. Ed.*, 2022, **61**, e202200120.
35 Y. Hong, W. Kim, T. Kim, C. Kaufmann, H. Kim, F. Würthner and D. Kim, Real-time Observation of Structural Dynamics Triggering Excimer Formation in a Perylene Bisimide Folda-dimer by Ultrafast Time-Domain Raman Spectroscopy, *Angew. Chem., Int. Ed.*, 2022, **61**, e202114474.
36 Y. Hong, J. Kim, W. Kim, C. Kaufmann, H. Kim, F. Würthner and D. Kim, Efficient Multiexciton State Generation in Charge-Transfer-Coupled Perylene Bisimide Dimers via Structural Control, *J. Am. Chem. Soc.*, 2020, **142**, 7845–7857.
37 E. Kirchner, D. Bialas, F. Fennel, M. Grüne and F. Würthner, Defined Merocyanine Dye Stacks from a Dimer up to an Octamer by Spacer-Encoded Self-Assembly Approach, *J. Am. Chem. Soc.*, 2019, **141**, 7428–7438.
38 A.-B. Bornhof, A. Bauzá, A. Aster, M. Pupier, A. Frontera, E. Vauthey, N. Sakai and S. Matile, Synergistic Anion–(π)n–π Catalysis on π-Stacked Foldamers, *J. Am. Chem. Soc.*, 2018, **140**, 4884–4892.
39 D. Bialas, A. Zitzler-Kunkel, E. Kirchner, D. Schmidt and F. Würthner, Structural and quantum chemical analysis of exciton coupling in homo- and heteroaggregate stacks of merocyanines, *Nat. Commun.*, 2016, **7**, 12949.
40 V. Dehm, M. Büchner, J. Seibt, V. Engel and F. Würthner, Foldamer with a spiral perylene bisimide staircase aggregate structure, *Chem. Sci.*, 2011, **2**, 2094–2100.
41 S. Bhosale, A. L. Sisson, P. Talukdar, A. Fürstenberg, N. Banerji, E. Vauthey, G. Bollot, J. Mareda, C. Röger, F. Würthner, N. Sakai and S. Matile, Photoproduction of Proton Gradients with π-Stacked Fluorophore Scaffolds in Lipid Bilayers, *Science*, 2006, **313**, 84–86.

42 R. S. Lokey and B. L. Iverson, Synthetic molecules that fold into a pleated secondary structure in solution, *Nature*, 1995, **375**, 303–305.
43 A. Schulz, R. Fröhlich, A. Jayachandran, F. Schneider, M. Stolte, T. Brixner and F. Würthner, Panchromatic light-harvesting antenna by supramolecular exciton band engineering for heteromeric dye foldamer, *Chem*, 2024, **10**, 2887–2900.
44 X. Hu, A. Schulz, J. O. Lindner, M. Grüne, D. Bialas and F. Würthner, Folding and fluorescence enhancement with strong odd–even effect for a series of merocyanine dye oligomers, *Chem. Sci.*, 2021, **12**, 8342–8352.
45 X. Hu, J. O. Lindner and F. Würthner, Stepwise Folding and Self-Assembly of a Merocyanine Folda-Pentamer, *J. Am. Chem. Soc.*, 2020, **142**, 3321–3325.
46 A. Mohanty, V. P. Singh, C. M. Hussain, M. Dey, D. Ghosh, P. Mukhopadhyay and J. Dasgupta, An order of magnitude modulation of singlet fission rates in NDI cyclophanes by tuning inter-chromophoric electronic coupling, *Chem. Sci.*, 2025, **16**, 21368–21378.
47 J. Shukla, S. P. Bera, M. R. Ajayakumar, S. Konar and P. Mukhopadhyay, Water-Stable, Eight-electron Acceptor Drives Anion···Water Assisted Tunable Ionic Self-Assembly and Proton Conduction, *Chem. – Eur. J.*, 2024, **30**, e202401334.
48 D. Bansal, A. Kundu, V. P. Singh, A. K. Pal, A. Datta, J. Dasgupta and P. Mukhopadhyay, A highly contorted push–pull naphthalenediimide dimer and evidence of intramolecular singlet exciton fission, *Chem. Sci.*, 2022, **13**, 11506–11512.
49 A. Mukherjee and S. Ghosh, Core-Substituted Naphthalene-Diimides (cNDI) and Related Derivatives: Versatile Scaffold for Supramolecular Assembly and Functional Materials, *Org. Mater.*, 2021, **3**, 405–416.
50 S. V. Bhosale, M. Al Kobaisi, R. W. Jadhav, P. P. Morajkar, L. A. Jones and S. George, Naphthalene diimides: perspectives and promise, *Chem. Soc. Rev.*, 2021, **50**, 9845–9998.
51 M. Al Kobaisi, S. V. Bhosale, K. Latham, A. M. Raynor and S. V. Bhosale, Functional Naphthalene Diimides: Synthesis, Properties, and Applications, *Chem. Rev.*, 2016, **116**, 11685–11796.
52 F. Würthner, S. Ahmed, C. Thalacker and T. Debaerdemaeker, Core-Substituted Naphthalene Bisimides: New Fluorophors with Tunable Emission Wavelength for FRET Studies, *Chem. – Eur. J.*, 2002, **8**, 4742–4750.
53 N. Sakai, R. Bhosale, D. Emery, J. Mareda and S. Matile, Supramolecular n/p-Heterojunction Photosystems with Antiparallel Redox Gradients in Electron- and Hole-Transporting Pathways, *J. Am. Chem. Soc.*, 2010, **132**, 6923–6925.
54 N. Sakai, A. L. Sisson, T. Bürgi and S. Matile, Assembly of Photoactive Rigid-Rod Naphthalenediimide π-Stack Architectures on Gold Nanoparticles and Gold Electrodes, *J. Am. Chem. Soc.*, 2007, **129**, 15758–15759.
55 V. Gorteau, G. Bollot, J. Mareda, A. Perez-Velasco and S. Matile, Rigid Oligonaphthalenediimide Rods as Transmembrane Anion–π Slides, *J. Am. Chem. Soc.*, 2006, **128**, 14788–14789.
56 A.-J. Avestro, D. M. Gardner, N. A. Vermeulen, E. A. Wilson, S. T. Schneebeli, A. C. Whalley, M. E. Belowich, R. Carmieli, M. R. Wasielewski and J. F. Stoddart, Gated Electron Sharing Within Dynamic Naphthalene Diimide-Based Oligorotaxanes, *Angew. Chem., Int. Ed.*, 2014, **53**, 4442–4449.
57 Y. Wu, M. Frasconi, D. M. Gardner, P. R. McGonigal, S. T. Schneebeli, M. R. Wasielewski and J. F. Stoddart, Electron Delocalization in a Rigid Cofacial Naphthalene-1,8:4,5-bis(dicarboximide) Dimer, *Angew. Chem., Int. Ed.*, 2014, **53**, 9476–9481.
58 A. Mukherjee, S. Barman, A. Ghosh, A. Datta, A. Datta and S. Ghosh, A Hierarchical (Macro)molecular Assembly Assisted by Donor–Acceptor Charge-Transfer Interactions Exhibiting Room-Temperature Ferroelectricity, *Angew. Chem., Int. Ed.*, 2022, **61**, e202203817.
59 K. Jalani, A. D. Das, R. Sasmal, S. S. Agasti and S. J. George, Transient dormant monomer states for supramolecular polymers with low dispersity, *Nat. Commun.*, 2020, **11**, 3967.
60 M. R. Molla and S. Ghosh, Hydrogen-Bonding-Mediated Vesicular Assembly of Functionalized Naphthalene–Diimide-Based Bolaamphiphile and Guest-Induced Gelation in Water, *Chem. – Eur. J.*, 2012, **18**, 9860–9869.
61 A. Das, M. R. Molla, A. Banerjee, A. Paul and S. Ghosh, Hydrogen-Bonding Directed Assembly and Gelation of Donor–Acceptor Chromophores: Supramolecular Reorganization from a Charge-Transfer State to a Self-Sorted State, *Chem. – Eur. J.*, 2011, **17**, 6061–6066.
62 A. Das and S. Ghosh, H-bonding directed programmed supramolecular assembly of naphthalene-diimide (NDI) derivatives, *Chem. Commun.*, 2016, **52**, 6860–6872.
63 A. Sarkar, R. Sasmal, C. Empereur-mot, D. Bochicchio, S. V. K. Kompella, K. Sharma, S. Dhiman, B. Sundaram, S. S. Agasti, G. M. Pavan and S. J. George, Self-Sorted, Random, and Block Supramolecular Copolymers via Sequence Controlled, Multicomponent Self-Assembly, *J. Am. Chem. Soc.*, 2020, **142**, 7606–7617.
64 A. Sarkar, T. Behera, R. Sasmal, R. Capelli, C. Empereur-mot, J. Mahato, S. S. Agasti, G. M. Pavan, A. Chowdhury and S. J. George, Cooperative Supramolecular Block Copolymerization for the Synthesis of Functional Axial Organic Heterostructures, *J. Am. Chem. Soc.*, 2020, **142**, 11528–11539.
65 H. Kar, D. W. Gehrig, N. K. Allampally, G. Fernández, F. Laquai and S. Ghosh, Cooperative supramolecular polymerization of an amine-substituted naphthalene-diimide and its impact on excited state photophysical properties, *Chem. Sci.*, 2016, **7**, 1115–1120.
66 S. K. Keshri, T. Ishizuka, T. Kojima, Y. Matsushita and M. Takeuchi, Long-Range Order in Supramolecular π Assemblies in Discrete Multidecker Naphthalenediimides, *J. Am. Chem. Soc.*, 2021, **143**, 3238–3244.
67 A. Das and S. Ghosh, Supramolecular Assemblies by Charge-Transfer Interactions between Donor and Acceptor

Chromophores, *Angew. Chem., Int. Ed.*, 2014, **53**, 2038–2054.
68 S. V. Bhosale, C. H. Jani and S. J. Langford, Chemistry of naphthalene diimides, *Chem. Soc. Rev.*, 2008, **37**, 331–342.
69 S. Basak, N. Nandi, A. Baral and A. Banerjee, Tailor-made design of J- or H-aggregated naphthalenediimide-based gels and remarkable fluorescence turn on/off behaviour depending on solvents, *Chem. Commun.*, 2015, **51**, 780–783.
70 T. D. M. Bell, S. V. Bhosale, C. M. Forsyth, D. Hayne, K. P. Ghiggino, J. A. Hutchison, C. H. Jani, S. J. Langford, M. A. P. Lee and C. P. Woodward, Melt-induced fluorescent signature in a simple naphthalenediimide, *Chem. Commun.*, 2010, **46**, 4881–4883.
71 M. Kumar and S. J. George, Green fluorescent organic nanoparticles by self-assembly induced enhanced emission of a naphthalene diimide bolaamphiphile, *Nanoscale*, 2011, **3**, 2130–2133.
72 F. Würthner, Dipole–Dipole Interaction Driven Self-Assembly of Merocyanine Dyes: From Dimers to Nanoscale Objects and Supramolecular Materials, *Acc. Chem. Res.*, 2016, **49**, 868–876.
73 C. Kaufmann, W. Kim, A. Nowak-Król, Y. Hong, D. Kim and F. Würthner, Ultrafast Exciton Delocalization, Localization, and Excimer Formation Dynamics in a Highly Defined Perylene Bisimide Quadruple π-Stack, *J. Am. Chem. Soc.*, 2018, **140**, 4253–4258.
74 N. J. Hestand and F. C. Spano, Expanded Theory of H- and J-Molecular Aggregates: The Effects of Vibronic Coupling and Intermolecular Charge Transfer, *Chem. Rev.*, 2018, **118**, 7069–7163.
75 C. Kaufmann, D. Bialas, M. Stolte and F. Würthner, Discrete π-Stacks of Perylene Bisimide Dyes within Folda-Dimers: Insight into Long- and Short-Range Exciton Coupling, *J. Am. Chem. Soc.*, 2018, **140**, 9986–9995.
76 P. Spenst, R. M. Young, B. T. Phelan, M. Keller, J. Dostál, T. Brixner, M. R. Wasielewski and F. Würthner, Solvent-Templated Folding of Perylene Bisimide Macrocycles into Coiled Double-String Ropes with Solvent-Sensitive Optical Signatures, *J. Am. Chem. Soc.*, 2017, **139**, 2014–2021.
77 C. Kulkarni, G. Periyasamy, S. Balasubramanian and S. J. George, Charge-transfer complexation between naphthalene diimides and aromatic solvents, *Phys. Chem. Chem. Phys.*, 2014, **16**, 14661–14664.
78 D. B. Hibbert and P. Thordarson, The death of the Job plot, transparency, open science and online tools, uncertainty estimation methods and other developments in supramolecular chemistry data analysis, *Chem. Commun.*, 2016, **52**, 12792–12805.
79 P. Spenst and F. Würthner, A Perylene Bisimide Cyclophane as a "Turn-On" and "Turn-Off" Fluorescence Probe, *Angew. Chem., Int. Ed.*, 2015, **54**, 10165–10168.
80 H. M. Colquhoun, E. P. Goodings, J. M. Maud, J. F. Stoddart, J. B. Wolstenholme and D. J. Williams, The complexation of the diquat dication by dibenzo-3n-crown-n ethers, *J. Chem. Soc., Perkin Trans. 2*, 1985, 607–624.